Published in final edited form as:
ACS Chem Biol. 2013 July 19; 8(7): 1519–1527. doi:10.1021/cb400158t.

Evidence for a functionally relevant rocaglamide binding site on the eIF4A:RNA complex

Heather Sadlish[1,*], **Gabriela Galicia-Vazquez**[3], **C. Gregory Paris**[2], **Thomas Aust**[1], **Bhupinder Bhullar**[1], **Lena Chang**[1], **Stephen B. Helliwell**[1], **Dominic Hoepfner**[1], **Britta Knapp**[1], **Ralph Riedl**[1], **Silvio Roggo**[1], **Sven Schuierer**[1], **Christian Studer**[1], **John A. Porco Jr.**[6], **Jerry Pelletier**[3,4,5], and **N. Rao Movva**[1]

[1]Novartis Institutes for BioMedical Research, Novartis Campus, CH-4056 Basel Switzerland [2]Novartis Institutes for BioMedical Research, 250 Massachusetts Avenue Cambridge MA 02139, United States of America [3]Department of Biochemistry, McGill University, Montreal, Quebec, Canada [4]Department of Oncology, McGill University, Montreal, Quebec, Canada [5]The Rosalind and Morris Goodman Cancer Research Center, McGill University, Montreal, Quebec, Canada [6]Department of Chemistry, Center for Chemical Methodology and Library Development, Boston University, Boston, Massachusetts, United States of America

Abstract

Translation initiation is an emerging target in oncology and neurobiology indications. Naturally derived and synthetic rocaglamide scaffolds have been used to interrogate this pathway, however, there is uncertainty regarding their precise mechanism(s) of action. We exploited the genetic tractability of yeast to define the primary effect of both a natural and a synthetic rocaglamide in a cellular context, and characterized the molecular target using biochemical studies and *in silico* modeling. Chemogenomic profiling and mutagenesis in yeast identified the eIF (eukaryotic Initiation Factor) 4A helicase homologue as the primary molecular target of rocaglamides, and defined a discrete set of residues near the RNA binding motif which confer resistance to both compounds. Three of the eIF4A mutations were characterized regarding their functional consequences on activity and response to rocaglamide inhibition. These data support a model whereby rocaglamides stabilize an eIF4A-RNA interaction to either alter the level and/or impair the activity of the eIF4F complex. Furthermore, *in silico* modeling supports the annotation of a binding pocket delineated by the RNA substrate and the residues identified from our mutagenesis screen. As expected from the high degree of conservation of the eukaryotic translation pathway, these observations are consistent with previous observations in mammalian model systems. Importantly, we demonstrate that the chemically distinct silvestrol and synthetic rocaglamides share a common mechanism of action, which will be critical for optimization of physiologically stable derivatives. Finally, these data confirm the value of the rocaglamide scaffold for exploring the impact of translational modulation on disease.

Introduction

Protein synthesis is a highly regulated process, and recent advances in our understanding have led to a growing awareness of its depth and complexity [1–3]. There are opportunities to modulate disease through selective inhibition of these processes, but a careful dissection of the role of translation in a given model system is required. This can be achieved with a

[*]Corresponding author: heather.sadlish@novartis.com.

Supporting Information: This material is available on http://pubs.acs.org.

variety of small molecules that have been described to modulate various nodes of the translation process, although an understanding of the precise mechanism of action is critical for interpretation [3, 4].

The family of cyclopenta[b]benzofuran natural products, which includes rocaglamides and silvestrol, have been isolated from numerous *Aglaia* species [5, 6]. Although silvestrol has demonstrated anti-tumor activity in a variety of cellular and murine models [7–11], the need to circumvent potential liabilities regarding its clinical applications [12, 13] has led to the generation of a wide array of synthetic derivatives [14–16]. Several of these synthetic compounds have been tested alongside silvestrol in a variety of *in vitro* assays, and while they appear to have similar properties [9, 12, 17], different molecular targets have been proposed [9, 18, 19].

The cyclopenta[b]benzofuran compounds have been shown to inhibit protein synthesis with little effect on DNA or RNA synthesis [5, 6, 8], however, the means of translational inhibition are unclear. Silvestrol has been reported to inhibit translation initiation by stimulating an interaction of RNA with the eIF4A helicase [8, 9]. eIF4A, together with the mRNA cap-binding eIF4E, and a scaffolding protein, eIF4G, are the three core components of the eIF4F complex. This complex is required for cap-dependent ribosome recruitment to mRNA templates during the initiation phase of translation, and non-specific sequestration of eIF4A to RNA by silvestrol is proposed to lead to translational arrest [9]. However, an alternative mechanism of action to explain the translation inhibition by synthetic rocaglamide derivatives has been proposed. Through disruption of c-RAF binding to prohibitin, the compounds are suggested to inhibit mitogen and extracellular-signal regulated protein kinase (MEK and ERK) signaling pathways to prevent eIF4E phosphorylation and subsequently suppress translation [18–21].

In this study, we aimed to define the primary molecular target and mechanism of action of a synthetic rocaglamide, ROC-N, and compared it to that of silvestrol. We utilized unbiased genome-wide assays with genetically tractable yeast, where the essential eukaryotic pathways are highly conserved. Two independent approaches highlighted the role of the eIF4A yeast homologue, TIF1, in mediating resistance to ROC-N. Further biochemical characterization confirmed that specific amino acids near the RNA binding site of TIF1 are critical for compound activity, but not protein function. *In silico* modeling places these residues in a pocket formed by the eIF4A:RNA complex. Taken together, our results demonstrate that silvestrol and the synthetic rocaglamide (ROC-N) exert identical means of inhibiting the helicase component of the eIF4F complex.

Results and Discussion

Haploinsufficiency Profiling Identifies Translation as a Rocaglamide Target

We used a yeast-based chemogenomic profiling technology as an unbiased approach to define the mechanism of action for rocaglamides in a cellular context. This assay exploits the conservation of essential biological pathways in eukaryotes, the genetic tractability of yeast, and takes advantage of a recently implemented robust automated platform to profile nearly 2000 compounds [22]. In this approach, a pool of ~6000 haploinsufficient strains covering the genome is treated with the compound of interest and the relative abundance of each strain determined. The sensitivity of each strain to the individual compound is plotted relative to the statistical sensitivity of that strain across thousands of chemically diverse scaffolds (z-score). In the simple case of a classic enzymatic inhibitor, the single strain in the pool that is haploinsufficient for the molecular target of that compound will be more sensitive, and show a growth disadvantage.

We profiled two rocaglamides: silvestrol and ROC-N, a derivative that lacks the dioxane moiety unique to silvestrol, but resembles many of the potent synthetic scaffolds examined in *in vitro* assays [8, 12, 17](Figure 1A). There is roughly 100-fold difference in the compound potencies in both the wild-type yeast used in the haploinsufficiency assay and in a Δ7 strain used in subsequent assays (see below; Figure 1B). The dioxanyl ring appears to reduce permeability of silvestrol across the yeast cell wall, as a derivative lacking only the ring is at least twice as potent in yeast (data not shown). We also confirmed that ROC-N inhibited expression of an inducible luciferase reporter in wild-type yeast (Figure 1C).

The haploinsufficiency profile for ROC-N is shown together with a comparison of the ROC-N and silvestrol z-scores (Figure 1D, E and Supplemental Table 1). The compounds have remarkably similar profiles, with numerous strains heterozygous for various components of the translation initiation pathway (eIF1A, eIF2, eIF3 and eIF5) being significantly sensitive. In contrast, strains haploinsufficient for components of the eIF4F complex leads to compound resistance. The relative resistance of the eIF4A (TIF1/2) strains is highly significant, as their positive z-score indicate they are unaffected by nearly 2000 unrelated compounds. Although the precise molecular targets cannot be defined from such a profile, it is clear that both silvestrol and ROC-N have similar modes of action involving inhibition of translation initiation in a cellular environment.

eIF4A is a Genetic Modifier of Rocaglamide Sensitivity

Distinct from the haploinsufficiency profiling, genome-wide mutagenesis in yeast is another unbiased approach for defining the precise mechanism of action of a given compound. Haploid mutants resistant to ROC-N were selected from a randomly mutagenized yeast pool plated on lethal doses of the compound. Genome sequencing of the resistant clones was used to identify commonly mutated ORFs within defined complementation groups. We identified resistant alleles from three complementation groups (A, A2 and B), that were subsequently validated upon demonstration that re-introduction of the wild-type gene restored sensitivity (Figure 2).

Complementation groups A and B were clearly distinct; however, there was an intermediate level of complementation between group A and A2 at low concentrations of compound (data not shown). Consistent with this partial complementation, group A and A2 carried mutations in two of the three components of the eIF4F complex: eIF4G1 (TIF4631) and eIF4A (TIF1/2) respectively. Group B yielded a single point mutation in Xrn1 (KEM1), an evolutionarily-conserved 5'-3' exonuclease component of cytoplasmic processing (P) bodies involved in mRNA decay. The resistance to ROC-N could be replicated through deletion of the KEM1 and TIF4631 genes in the parental haploid strain, suggesting that these two mutations likely resulted in a loss-of-function of the respective protein (Figure 2B). These data are independent confirmation of the observed resistance of the TIF1/2 and TIF4631 deletion strains in the haploinsufficiency profiling assay, and clearly indicate that the inhibition of translation initiation is primarily mediated through the eIF4F complex.

Yeast express duplicated forms of the eIF4G (TIF4631/4632) and eIF4A (TIF1/2) genes with overlapping functional roles. Deletion of TIF4631 but not TIF4632 has an effect on global translation rates, suggesting these isoforms have somewhat different roles [23]. The TIF1/2 isoforms, however, are identical at the amino acid level and have no apparent functional difference [24]. Thus, the identified mutations in TIF1/2 appear to behave dominantly. Further, the ability to restore compound sensitivity by re-introduction of the wild-type gene from a plasmid demonstrates that the identified TIF1/2 mutations are necessary and sufficient for conferring resistance to compound, and illustrates the importance of TIF1/ 2 gene dosage.

The identification of dominant resistant alleles in TIF1/2 provides direct evidence that rocaglamides target the helicase, and is consistent with reports showing that silvestrol stimulates association of the mammalian eIF4A protein and RNA [8, 9]. Although these experiments do not rule out the possibility that rocaglamides target other cellular proteins, taken together they clearly indicate that the eIF4F complex, and in particular, eIF4A (TIF1/2), has a significant role in the mechanism of action. To validate and extend these findings, we performed random mutagenesis of the TIF1 ORF *in vitro*. The mutant library was introduced into a haploid yeast strain lacking TIF2 (Δ*tif2*) via homologous recombination, such that the sole copy of the eIF4A protein was randomly mutated. Thus, transformants capable of growing in lethal concentrations of ROC-N presumably carry a resistant allele of TIF1 that must also fulfill its normal essential role [24]. We identified twelve unique alterations, all of which mapped to 6 amino acids clustering near the RNA binding motif of TIF1 (Table 1, Figure 7A, see below for further analysis). Figure 3 summarizes the growth advantage of the individual mutants over the parental wild-type and Δ*tif2* strains in lethal concentrations of ROC-N and silvestrol. Importantly, the mutated strains demonstrate a similar pattern of sensitivity to both compounds, suggesting a common means of interaction with the TIF1 protein.

Functional Consequences of ROC-N-resistant TIF1 Mutations

To directly assess the consequences of the ROC-N-resistant TIF1 mutations on the different functional roles of the protein, we chose representatives of the most frequently altered sites (P147Q, F151L, Q183E) for further biochemical characterization. The TIF1 mutations had no discernible consequences on protein expression or stability, and were purified from *E. coli* to ~ 95% homogeneity (Figure 4A).

eIF4A is an RNA-dependent ATPase driven helicase, where both RNA binding and ATP hydrolysis are required for helicase activity [25, 26]. Due to the localization of the mutated amino acids near the RNA binding motif, we first evaluated whether the RNA-binding capacity of the mutant proteins was altered used a filter-binding assay (Figure 4B). Similar levels of ATP-stimulated binding to a model RNA template was observed for both wild-type and mutant TIF1 proteins, indicating that the mutations do not significantly impact RNA binding *per se* under these conditions. Addition of ROC-N or silvestrol stimulated wild-type protein binding ~ 3–4 fold, as previously reported for mammalian eIF4A [9]. None of the three TIF1 mutant proteins, however, displayed increased RNA binding upon treatment with ROC-N or silvestrol but rather showed binding similar to that in the absence of compound (+ATP lanes). Thus, while the mutated TIF1 proteins can bind RNA to levels similar to wild-type protein, the ability of both silvestrol and ROC-N to enhance this interaction is blocked.

We next assessed the ATPase activity of the respective TIF1 mutant proteins (Figure 5). A time course assay indicated that all mutants were capable of hydrolyzing ATP, although there were slight differences in kinetics. TIF1-P147Q and TIF1-Q183E showed similar ATPase activity as wild-type, whereas TIF1-F151L displayed a slightly higher rate of hydrolysis (nearly 2-fold). The addition of both silvestrol and ROC-N stimulated wild-type TIF1 ATPase activity by more than 2-fold throughout the course of the assay, consistent with the compound-mediated increase in protein:RNA interaction. In contrast, neither compound stimulated the ATPase activity of any of the three mutants, and there was even some inhibition observed for the TIF1-F151L and TIF1-P147Q mutants.

Finally, we evaluated the helicase activity of the wild-type and mutant TIF1 proteins on a model RNA duplex (Figure 6A). The mutated proteins were able to unwind the substrate similar to wild-type in the absence of compound, although the TIF1-Q183E mutation was ~2-fold less active (Figure 6B). The addition of ROC-N and silvestrol stimulated wild-type

TIF1 helicase activity and is consistent with the increased ATPase activity upon compound treatment (Figure 5). All three TIF1 mutants were recalcitrant to the stimulatory effects of ROC-N or silvestrol (Figure 6C), with the helicase activity of the TIF1-F151L and TIF1-Q183E proteins remaining unaltered as compared to vehicle treated samples and that ofTIF1-P147Q slightly inhibited by silvestrol (Figure 6C). Taken together, these results identify P147Q, F151L, and Q183E as amino acid changes that do not affect the essential activities of the TIF1 protein, but are capable of uncoupling the effects of ROC-N and silvestrol on TIF1 activity *in vitro*.

In silico analysis indicates a druggable pocket at the eIF4A:RNA interface

We thought it remarkable that all resistant alleles identified in the mutagenesis screen were localized to only six residues of the eIF4A helicase. *In silico* analysis was used to map the sites onto crystal structures of TIF1/2 and the related (61% identical) human eIF4AIII helicase which was generated with a ssRNA substrate (Figure 7A)[27, 28]. As expected from this highly conserved helicase family, the secondary and tertiary features of these two proteins are closely aligned. Further, we observed that all six identified mutant residues are in close proximity to each other, and to the RNA binding site. Further analysis with SiteMap software permitted the identification of invaginations (pockets) on the protein surface. These pockets are computationally ranked by geometric and physico-chemical properties (SiteScore) and the predicted ability to bind a drug-like small molecule (DScore).

A cluster of linked pockets was identified in the eIF4AIII D1 sub-domain in proximity to the bound ssRNA, between the alpha-4 and alpha-3 helices (Figure 7B). The DScore value for this complex site is considered druggable, and reflects the probability that a small molecule such as ROC-N or silvestrol could bind. The central sub-site is highly hydrophobic, and lies directly in contact with the homologs of the TIF1/2 mutated residues, Q183 and F151. There are two smaller sub-sites including a polar cleft overlaying the RNA and another extending up toward the beta-5 strand that is mixed hydrophobic and hydrophilic. Although the central sub-site can be identified in both eIF4AIII and TIF1/2 structures where the RNA is absent, the considerably lower DScore values indicates little probability of a binding pocket (data not shown). Thus, we propose that the rocaglamide binding pocket is bounded by residues identified in the mutagenesis screen, and the RNA substrate. This would provide an explanation for the observation that the compounds enhance the interaction between TIF1 and RNA (Figure 4) to stimulate the ATPase and subsequent helicase activity of the protein (Figures 5 and 6). The rocaglamide binding pocket formed by the eIF4A:RNA complex is reminiscent of “interfacial inhibition” demonstrated by other natural products including camptothecin and brefeldin [29]. In these examples, the small molecule binds a transient interface formed by protein:protein or protein:nucleic acid interactions. Further, the complex and dynamic nature of these pockets provides a potential for specificity of inhibition [30].

Taken together, these data support a model whereby rocaglamides lock TIF1/2 onto RNA, leading to an initial increase in helicase activity, but ultimately resulting in translational inhibition. The effect on initiation may be due to depletion of eIF4A from the eIF4F complex, if eIF4A is sequestered non-specifically to RNA. Another non- mutually exclusive possibility is that the compounds alter the interaction of the eIF4F complex with target mRNAs. Haploinsufficiency of TIF1/2 may lead to rocaglamide resistance (Figure 1) by decreasing the TIF1/2 target pool that would interfere with eIF4F function, consistent with a dominant or gain-of-function mechanism of inhibition. Yeast may be particularly suited to identify this mechanism of action given that reduced TIF1 levels are sufficient to support translation initiation [24].

Rocaglamides have also been reported to bind to Prohibitins (PHB) 1 and 2, blocking their interaction with cRaf, and leading to inhibition of Raf-MEK-ERK signaling [18]. This is

unlikely to be the mechanism responsible for inhibition of translation by rocaglamides since these compounds are active in translation extracts where these signaling pathways are not intact [8]. Further, the Raf-MEK-ERK pathway signals to Mnk 1/2, which in turn phosphorylates eIF4E. However, while elimination of Mnk1/2 in the mouse germline abolishes eIF4E phosphorylation, it does not affect global translation rates [31]. Additionally, while the yeast prohibitin homologues share 55% identity with the human protein, the growth of the haploinsufficient strains is unaffected by ROC-N or silvestrol, suggesting that they are not the primary target in a cellular context (Supplemental Table S1). On the other hand, the identification of TIF1/2 as the rocaglamide target is consistent with studies in mammalian model systems which have documented silvestrol effects on eIF4F-dependent translation events [8–10, 12, 17]. Further, a recent *in vitro* study identified mammalian eIF4AI/II as a target for biotinylated episilvestrol and silvestrol [32], consistent with our observations.

In addition to identifying the primary molecular target, we provide strong evidence for a putative rocaglamide binding site comprised of the eIF4A protein and the RNA substrate. We have also demonstrated that a synthetic rocaglamide derivative inhibits eIF4A through a similar mechanism as the silvestrol natural product. This is of particular interest as silvestrol has been observed to have limited stability in some *in vivo* systems and there is a need for developing analogues that can be generated by simpler synthetic routes and with improved pharmacological properties [12, 13]. Taken together, this work significantly improves upon our understanding of the mechanism behind rocaglamide inhibition of translation initiation, and will help future efforts targeting this pathway.

Methods

Compounds

The rocaglamide derivative, ROC-N (CAS# 394248-26-1: (1R,2R,3S,3aR,8bS) rel-3a-(4-bromophenyl)-1,8b-dihydroxy-N,6,8-trimethoxy-N-methyl-3-phenyl-2,3,3a,8b-tetrahydro-1H-cyclopenta[b]benzofuran-2-carboxamide), and silvestrol (CAS#697235-38-4) were synthesized according to published procedures [14, 16, 33, 34]. Compounds were dissolved in dimethyl sulfoxide (DMSO).

Haploinsufficiency assay

Yeast haploinsufficiency profiling was performed as previously published [35]. Specific assay adaptations concerning starting culture density, reaction culture volume, dilution scheme, and experimental controls have been described, as has details of data analysis [22].

The data matrices of the scores for the haploinsufficiency experiments are available (Supplementary Table S1). For each ROC-N and silvestrol there are columns with the MADL (sensitivity) or the z-score. Missing values are indicated by the empty string. Note that since the file contains rows for all ORFs, there are a number of rows that do not contain any measurement.

Luciferase assay

A haploid BY4741 strain carrying an integrated firefly luciferase under control of an inducible galactose promoter was used to assess compound effects on expression. Yeast in mid-logarithmic growth phase were treated with compound dilutions for 3 hours prior to quantification of luciferase gene product. Steady-Glo (Promega) was added to the cells, which were lysed using ultrasonication (Covaris-S series AFA, Covaris Inc) prior to detection on ViewLux.

Selection of drug resistant *S.cerevisiae* cells

Parental BY4741 strains deleted for 7 genes (Δ*7*) involved in drug resistance (*snq2::KanMX; pdr5::KanMX; pdr1::NAT1; pdr3::KanMX; yap1::NAT1; pdr2::LEU2; yrm1::MET*) were mutagenized by incubating with 2.5% ethylmethanesulfonate for 15 minutes or 30 minutes to obtain about 60–80% cell survival. A total of 1×10^7 mutagenized cells were plated on 14 cm^2 dishes with synthetic complete medium (0.7 g/l Difco Yeast Nitrogen Base w/o amino acids, 0.79 g/l MPbio CSM amino acid mixture, 2% Glucose) containing the corresponding growth inhibitory concentration of compound. Resistant colonies usually appeared after 2–4 days and resistance was confirmed by re-streaking. Stable resistant colonies were mated as appropriate to determine complementation groups. Genomic DNA was prepared using Qiagen Tip100 (Qiagen), quantified using Qubit Fluorometric quantitation (Life Technologies), then 5 μg of DNA was fragmented using ultrasonication to 200 bp (Covaris-S series AFA, Covaris Inc). The library was prepared for sequencing using Illumina Solexa Paired End −36 (PE36) kit (Illumina Corp.) according to the manufacturer' instructions. The raw sequence reads were aligned to the reference strain (S288C Reference Genome build R63-1-1_20100105) using BWA software. From comparison to the parental strain (BY4741Δ*7*) the SNPs were identified in potential target genes in the resistant strains.

Random mutagenesis of TIF1

A construct encoding the complete TIF1 ORF in the pRS413 backbone was randomly mutagenized using a degenerate PCR approach where reactions were performed under standard conditions, but contained 0.2–0.5 mM $MnSO_4$. The amplified product was purified by agarose gel electrophoresis, and transformed into a haploid BY4741Δ*7* strain lacking TIF2 (Δ*7*; *tif2::LYS*). Through homologous recombination, the only remaining copy of TIF1 was replaced by the mutated variant. Resistant transformants were selected and confirmed as described above. To identify the resistant mutation, the TIF1 ORF was amplified from genomic DNA isolated from the resistant mutants, and sequenced using standard conditions.

Generation and Purification of Recombinant TIF1 Proteins

TIF1 mutants (nucleotides 217 to 1188; GenBank ID: NM 001179849.3) were synthesized *de novo* by GenScript and cloned into the AgeI/BamHI sites of pET15b/His_6-TIF1. Recombinant proteins were expressed and purified by Ni+2-NTA agarose chromatography as previously described [36]. The imidazole eluents were dialyzed against Buffer A overnight (20 mM Tris–HCl [pH 7.5], 10% glycerol, 100 mM KCl, 0.1 mM EDTA, and 2 mM DTT), aliquoted, and stored at −80°C.

RNA Binding Assays

Filter binding assays were performed as previously described [37]. Essentially, ^{32}P-labeled CAT mRNA was generated by linearization of pSP/CAT with PvuII and used in an *in vitro* transcription reaction. The radiolabeled mRNA was incubated with 1.5 μg of protein in Binding Buffer (25mM Tris HCl [pH 7.5], 1 mM DTT, 100 mM KCl, 5 mM $MgCl_2$, supplemented with 3.5 μg of BSA) in the presence of 2 mM ATP (unless otherwise indicated) and 0.5% DMSO or compound in a final volume of 50 μl. Reactions were at 37oC for 10 minutes, after which they were applied to nitrocellulose filters (pre-blocked with 0.1 % sodium pyrophosphate), washed, and dried. The amount of mRNA retained on the filters was determined by scintillation counting using a Beckman Coulter LS6500 Scintillation Counter.

ATPase Assays

ATPase assays were performed as previously described [36]. Essentially, 1 μg of wt TIF1 or TIF1 mutant was incubated for 1 h in the presence of 0.5% DMSO or the indicated amount of rocaglamide in 2.5 mM $MgCl_2$, 1 mM DTT, 1% glycerol, 20 mM MES–KOH [pH 6], and 10 mM KOAc, 2.5 μM poly(U) and 1 μM γ-^{32}P-ATP (10 Ci/mmol) in a 20 μl reaction. Incubations were performed at 25°C and aliquots taken at various time points were terminated by the addition of EDTA to a final concentration of 12.5 μM. Samples were spotted onto PEI cellulose F TLC plates (Merck) and developed in 0.3 M NaH_2PO_4 / 1 M LiCl.

RNA Helicase Assays

The generation of duplex substrate and RNA helicase assays were performed as previously described [38]. Essentially, 2 nM duplex RNA containing one radiolabeled strand was incubated with 0.36 μg wild-type TIF1 or mutant TIF1 in 20 mM HEPES [pH 7.5], 70 mM KCl, 2 mM DTT, 1 mM $Mg(OAc)_2$, 1 mM ATP and 20 μg acetylated BSA (Ambion) in a 20 μl reaction for 15 min at 35°C. Reactions are stopped with 5 μl stop solution (50% glycerol, 2% SDS, 20 μM EDTA, Bromophenol Blue and Xylene Cyanol dyes) and immediately loaded onto a 12% polyacrylamide gel (pre-run 30 min at 200 V in 1 × TBE at 4 °C). Electrophoresis was performed for 2–2.5 h at 200V in 1 × TBE at 4°C, the gel dried, subjected to autoradiography and quantified using a Typhoon Scanner. Student t-test was performed using GraphPad InStat version 3.10 (San Diego).

In silico modeling

Structures of human eIF4AIII were co-crystallized with RNA substrate and AMPPNP (PDB 2HYI) or without (PDB2HXY) [27]. Structures of TIF1/2 included 2VSO and 2VSX [28]; both were co-crystalized with AMP but no RNA substrate. Protein pocket discovery, computation and scoring was conducted by SiteMap version 2.6 (2012, Schrodinger: New York, NY; [39]). This version of SiteMap includes a user interface switch to “detect shallow binding sites” which relaxes the parameters for pocket depth (enclosure 0.4; maxvdw 0.55) and extends the parameters for pocket-to-pocket merger (dthresh 6.5; rthresh 5.0), while leaving unaltered the parameters governing pocket scoring for both SiteScore and DScore metrics. These “shallow” options were used during this work due to the shallow nature of the pockets in question; the helicase pockets described here were also detected with earlier versions of SiteMap using unedited parameters, but were not merged into a single, scorable site. Helicase sequence alignment was aided by the family alignment of [40]. 3D structure alignment of helicase D1 domains was conducted in ICM version 3.7-2d (2012, Molsoft: San Diego, CA: [41]) using default parameters (sequence-weight 0.5; seed-length 15). Graphical visualization is presented either in Maestro version 9.3 (2012, Schrodinger: New York, NY) or ICM version 3.7-2d (2012, Molsoft: San Diego, CA). Canonical nomenclature for helicase secondary structure features are derived from [42].

Supplementary Material

Refer to Web version on PubMed Central for supplementary material.

Acknowledgments

G. Galicia-Vazquez is supported by a Cole Foundation Fellowship, and was also supported by a CIHR Strategic Training Initiative in Chemical Biology. Part of this work was supported by the Canadian Institutes of Health Research (MOP-106530 to J. Pelletier) and the National Institutes of Health (GM073855 to J. A. Porco Jr.).

Reference List

1. Hinnebusch AG, Lorsch JR. The mechanism of eukaryotic translation initiation: new insights and challenges. Cold Spring Harb. Perspect. Biol. 2012; 4
2. Grech G, von LM. The role of translation initiation regulation in haematopoiesis. Comp Funct. Genomics. 2012; 2012:576540. [PubMed: 22649283]
3. Silvera D, Formenti SC, Schneider RJ. Translational control in cancer. Nat. Rev. Cancer. 2010; 10:254–266. [PubMed: 20332778]
4. Blagden SP, Willis AE. The biological and therapeutic relevance of mRNA translation in cancer. Nat. Rev. Clin. Oncol. 2011; 8:280–291. [PubMed: 21364523]
5. Lee SK, Cui B, Mehta RR, Kinghorn AD, Pezzuto JM. Cytostatic mechanism and antitumor potential of novel 1H-cyclopenta[b]benzofuran lignans isolated from Aglaia elliptica. Chem. Biol. Interact. 1998; 115:215–228. [PubMed: 9851291]
6. Ohse T, Ohba S, Yamamoto T, Koyano T, Umezawa K. Cyclopentabenzofuran lignan protein synthesis inhibitors from Aglaia odorata. J. Nat. Prod. 1996; 59:650–652. [PubMed: 8759160]
7. Alinari L, Prince CJ, Edwards RB, Towns WH, Mani R, Lehman A, Zhang X, Jarjoura D, Pan L, Kinghorn AD, Grever MR, Baiocchi RA, Lucas DM. Dual targeting of the cyclin/Rb/E2F and mitochondrial pathways in mantle cell lymphoma with the translation inhibitor silvestrol. Clin. Cancer Res. 2012; 18:4600–4611. [PubMed: 22791882]
8. Bordeleau ME, Robert F, Gerard B, Lindqvist L, Chen SM, Wendel HG, Brem B, Greger H, Lowe SW, Porco JA Jr, Pelletier J. Therapeutic suppression of translation initiation modulates chemosensitivity in a mouse lymphoma model. J. Clin. Invest. 2008; 118:2651–2660. [PubMed: 18551192]
9. Cencic R, Carrier M, Galicia-Vazquez G, Bordeleau ME, Sukarieh R, Bourdeau A, Brem B, Teodoro JG, Greger H, Tremblay ML, Porco JA Jr, Pelletier J. Antitumor activity and mechanism of action of the cyclopenta[b]benzofuran, silvestrol. PLoS. One. 2009; 4:e5223. [PubMed: 19401772]
10. Lucas DM, Edwards RB, Lozanski G, West DA, Shin JD, Vargo MA, Davis ME, Rozewski DM, Johnson AJ, Su BN, Goettl VM, Heerema NA, Lin TS, Lehman A, Zhang X, Jarjoura D, Newman DJ, Byrd JC, Kinghorn AD, Grever MR. The novel plant-derived agent silvestrol has B-cell selective activity in chronic lymphocytic leukemia and acute lymphoblastic leukemia in vitro and in vivo. Blood. 2009; 113:4656–4666. [PubMed: 19190247]
11. Hwang BY, Su BN, Chai H, Mi Q, Kardono LB, Afriastini JJ, Riswan S, Santarsiero BD, Mesecar AD, Wild R, Fairchild CR, Vite GD, Rose WC, Farnsworth NR, Cordell GA, Pezzuto JM, Swanson SM, Kinghorn AD. Silvestrol and episilvestrol, potential anticancer rocaglate derivatives from Aglaia silvestris. J. Org. Chem. 2004; 69:3350–3358. [PubMed: 15132542]
12. Liu T, Nair SJ, Lescarbeau A, Belani J, Peluso S, Conley J, Tillotson B, O'Hearn P, Smith S, Slocum K, West K, Helble J, Douglas M, Bahadoor A, Ali J, McGovern K, Fritz C, Palombella VJ, Wylie A, Castro AC, Tremblay MR. Synthetic silvestrol analogues as potent and selective protein synthesis inhibitors. J. Med. Chem. 2012; 55:8859–8878. [PubMed: 23025805]
13. Saradhi UV, Gupta SV, Chiu M, Wang J, Ling Y, Liu Z, Newman DJ, Covey JM, Kinghorn AD, Marcucci G, Lucas DM, Grever MR, Phelps MA, Chan KK. Characterization of silvestrol pharmacokinetics in mice using liquid chromatography-tandem mass spectrometry. AAPS. J. 2011; 13:347–356. [PubMed: 21499689]
14. Dobler MR, Bruce I, Cederbaum F, Cooke NG, Diorazio LJ, Hall RG, Irving E. Total synthesis of (±)-rocaglamide and some aryl analogues. Tetrahedron Letters. 2001; 42:8281–8284.
15. Gerard B, Cencic R, Pelletier J, Porco JA Jr. Enantioselective synthesis of the complex rocaglate (-)-silvestrol. Angew. Chem. Int. Ed Engl. 2007; 46:7831–7834. [PubMed: 17806093]
16. Adams TE, El SM, Hawkins BC, Hirner S, Holloway G, Khoo ML, Owen DJ, Savage GP, Scammells PJ, Rizzacasa MA. Total synthesis of the potent anticancer Aglaia metabolites (-)-silvestrol and (-)-episilvestrol and the active analogue (-)-4'-desmethoxyepisilvestrol. J. Am. Chem. Soc. 2009; 131:1607–1616. [PubMed: 19140688]

17. Rodrigo CM, Cencic R, Roche SP, Pelletier J, Porco JA. Synthesis of rocaglamide hydroxamates and related compounds as eukaryotic translation inhibitors: synthetic and biological studies. J. Med. Chem. 2012; 55:558–562. [PubMed: 22128783]
18. Polier G, Neumann J, Thuaud F, Ribeiro N, Gelhaus C, Schmidt H, Giaisi M, Kohler R, Muller WW, Proksch P, Leippe M, Janssen O, Desaubry L, Krammer PH, Li-Weber M. The natural anticancer compounds rocaglamides inhibit the Raf-MEK-ERK pathway by targeting prohibitin 1 and 2. Chem. Biol. 2012; 19:1093–1104. [PubMed: 22999878]
19. Zhu JY, Lavrik IN, Mahlknecht U, Giaisi M, Proksch P, Krammer PH, Li-Weber M. The traditional Chinese herbal compound rocaglamide preferentially induces apoptosis in leukemia cells by modulation of mitogen-activated protein kinase activities. Int. J. Cancer. 2007; 121:1839–1846. [PubMed: 17565740]
20. Bleumink M, Kohler R, Giaisi M, Proksch P, Krammer PH, Li-Weber M. Rocaglamide breaks TRAIL resistance in HTLV-1-associated adult T-cell leukemia/lymphoma by translational suppression of c-FLIP expression. Cell Death. Differ. 2011; 18:362–370. [PubMed: 20706274]
21. Proksch P, Giaisi M, Treiber MK, Palfi K, Merling A, Spring H, Krammer PH, Li-Weber M. Rocaglamide derivatives are immunosuppressive phytochemicals that target NF-AT activity in T cells. J. Immunol. 2005; 174:7075–7084. [PubMed: 15905551]
22. Hoepfner D, Karkare S, Helliwell SB, Pfeifer M, Trunzer M, De BS, Zimmerlin A, Tao J, Richie D, Hofmann A, Reinker S, Frederiksen M, Movva NR, Porter JA, Ryder NS, Parker CN. An integrated approach for identification and target validation of antifungal compounds active against Erg11p. Antimicrob. Agents Chemother. 2012; 56:4233–4240. [PubMed: 22615293]
23. Clarkson BK, Gilbert WV, Doudna JA. Functional overlap between eIF4G isoforms in Saccharomyces cerevisiae. PLoS. One. 2010; 5:e9114. [PubMed: 20161741]
24. Linder P, Slonimski PP. An essential yeast protein, encoded by duplicated genes TIF1 and TIF2 and homologous to the mammalian translation initiation factor eIF-4A, can suppress a mitochondrial missense mutation. Proc. Natl. Acad. Sci. U.S.A. 1989; 86:2286–2290. [PubMed: 2648398]
25. Lorsch JR, Herschlag D. The DEAD box protein eIF4A. 1. A minimal kinetic and thermodynamic framework reveals coupled binding of RNA and nucleotide. Biochemistry. 1998; 37:2180–2193. [PubMed: 9485364]
26. Peck ML, Herschlag D. Effects of oligonucleotide length and atomic composition on stimulation of the ATPase activity of translation initiation factor elF4A. RNA. 1999; 5:1210–1221. [PubMed: 10496222]
27. Andersen CB, Ballut L, Johansen JS, Chamieh H, Nielsen KH, Oliveira CL, Pedersen JS, Seraphin B, Le HH, Andersen GR. Structure of the exon junction core complex with a trapped DEAD-box ATPase bound to RNA. Science. 2006; 313:1968–1972. [PubMed: 16931718]
28. Schutz P, Bumann M, Oberholzer AE, Bieniossek C, Trachsel H, Altmann M, Baumann U. Crystal structure of the yeast eIF4A-eIF4G complex: an RNA-helicase controlled by protein-protein interactions. Proc. Natl. Acad. Sci. U. S. A. 2008; 105:9564–9569. [PubMed: 18606994]
29. Pommier Y, Marchand C. Interfacial inhibitors: targeting macromolecular complexes. Nat. Rev. Drug Discov. 2012; 11:25–36. [PubMed: 22173432]
30. Pommier Y, Cherfils J. Interfacial inhibition of macromolecular interactions: nature's paradigm for drug discovery. Trends Pharmacol. Sci. 2005; 26:138–145. [PubMed: 15749159]
31. Ueda T, Watanabe-Fukunaga R, Fukuyama H, Nagata S, Fukunaga R. Mnk2 and Mnk1 are essential for constitutive and inducible phosphorylation of eukaryotic initiation factor 4E but not for cell growth or development. Mol. Cell Biol. 2004; 24:6539–6549. [PubMed: 15254222]
32. Chambers JM, Lindqvist LM, Webb A, Huang DC, Savage GP, Rizzacasa MA. Synthesis of Biotinylated Episilvestrol: Highly Selective Targeting of the Translation Factors eIF4AI/II. Org. Lett. 2013; 15:1406–1409. [PubMed: 23461621]
33. El Sous M, Khoo ML, Holloway G, Owen D, Scammells PJ, Rizzacasa MA. Total synthesis of (-)-episilvestrol and (-)-silvestrol. Angew. Chem. Int. Ed Engl. 2007; 46:7835–7838. [PubMed: 17823902]
34. Thuaud F, Bernard Y, Turkeri G, Dirr R, Aubert G, Cresteil T, Baguet A, Tomasetto C, Svitkin Y, Sonenberg N, Nebigil CG, Desaubry L. Synthetic analogue of rocaglaol displays a potent and

selective cytotoxicity in cancer cells: involvement of apoptosis inducing factor and caspase-12. J. Med. Chem. 2009; 52:5176–5187. [PubMed: 19655762]

35. Pierce SE, Davis RW, Nislow C, Giaever G. Genome-wide analysis of barcoded Saccharomyces cerevisiae gene-deletion mutants in pooled cultures. Nat. Protoc. 2007; 2:2958–2974. [PubMed: 18007632]
36. Cencic R, Galicia-Vazquez G, Pelletier J. Inhibitors of translation targeting eukaryotic translation initiation factor 4A. Methods Enzymol. 2012; 511:437–461. [PubMed: 22713332]
37. Merrick WC, Sonenberg N. Assays for eukaryotic translation factors that bind mRNA. Methods. 1997; 11:333–342. [PubMed: 9126548]
38. Rogers GW Jr, Richter NJ, Merrick WC. Biochemical and kinetic characterization of the RNA helicase activity of eukaryotic initiation factor 4A. J. Biol. Chem. 1999; 274:12236–12244. [PubMed: 10212190]
39. Halgren TA. Identifying and characterizing binding sites and assessing druggability. J. Chem. Inf. Model. 2009; 49:377–389. [PubMed: 19434839]
40. Fairman-Williams ME, Guenther UP, Jankowsky E. SF1 and SF2 helicases: family matters. Curr. Opin. Struct. Biol. 2010; 20:313–324. [PubMed: 20456941]
41. Abagyan RA, Totrov MM, Kuznetsov DA. ICM: A New Method for Protein Modeling and Design: Applications to Docking and Structure Prediction from the Distorted Native Conformation. Journal of Computational Chemistry. 1994; 15:488–506.
42. Caruthers JM, McKay DB. Helicase structure and mechanism. Curr. Opin. Struct. Biol. 2002; 12:123–133. [PubMed: 11839499]

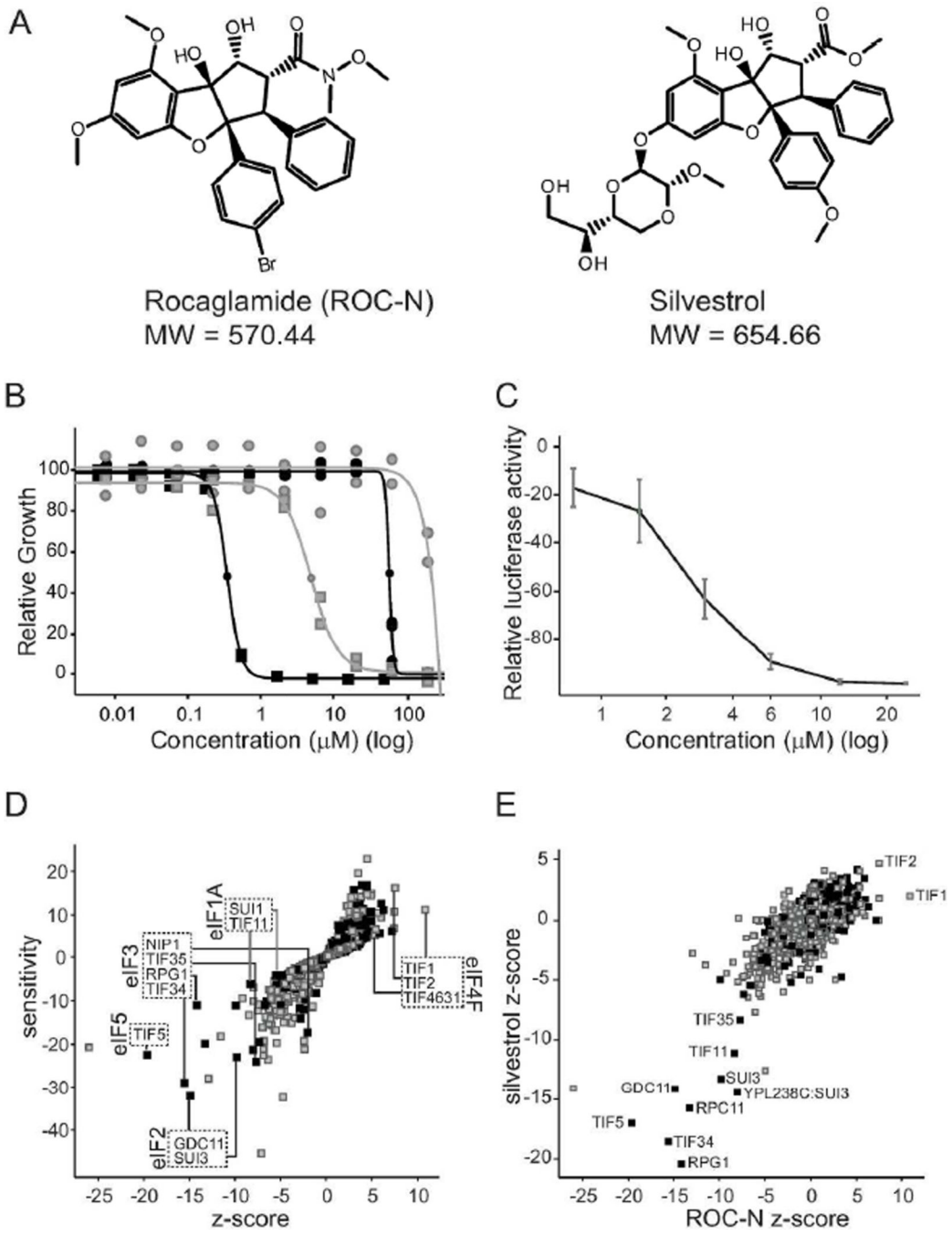

Figure 1.

Components of the translation initiation pathway alter the cellular response to rocaglamides. **A.** Chemical scaffolds examined in this study. **B.** Normalized growth (measured by OD600) of wild-type (gray) and Δ*7* (black) yeast strains in the presence of ROC-N (squares) and silvestrol (circles). Shown are biological and technical replicates. n = 2. **C.** ROC-N inhibits expression of a luciferase reporter. Luciferase levels relative to a DMSO control are plotted versus compound concentration (log). n=3 ± SEM **D.** Haploinsufficiency profile of ROC-N (6 μM) with relative strain sensitivity plotted as a function of statistical significance (z-score). Strains essential for viability (black) and non-essential (gray) are indicated. Deletion

strains involved in key translation initiation complexes are highlighted, together with the corresponding mammalian nomenclature annotated. **E.** Haploinsufficiency profile (z-score) of ROC-N (6 μM) is plotted as a function of silvestrol (200 μM). Commonly affected strains are highlighted.

A

Complementation Group	Clone	Mating Type	Mutation
A	1	a	TIF4631-Q345*
A2	4	a	TIF2-Q183K
A2	9	α	TIF2-Q183L
A2	11	α	TIF1-P147L
B	6	a	KEM1-G2C

B

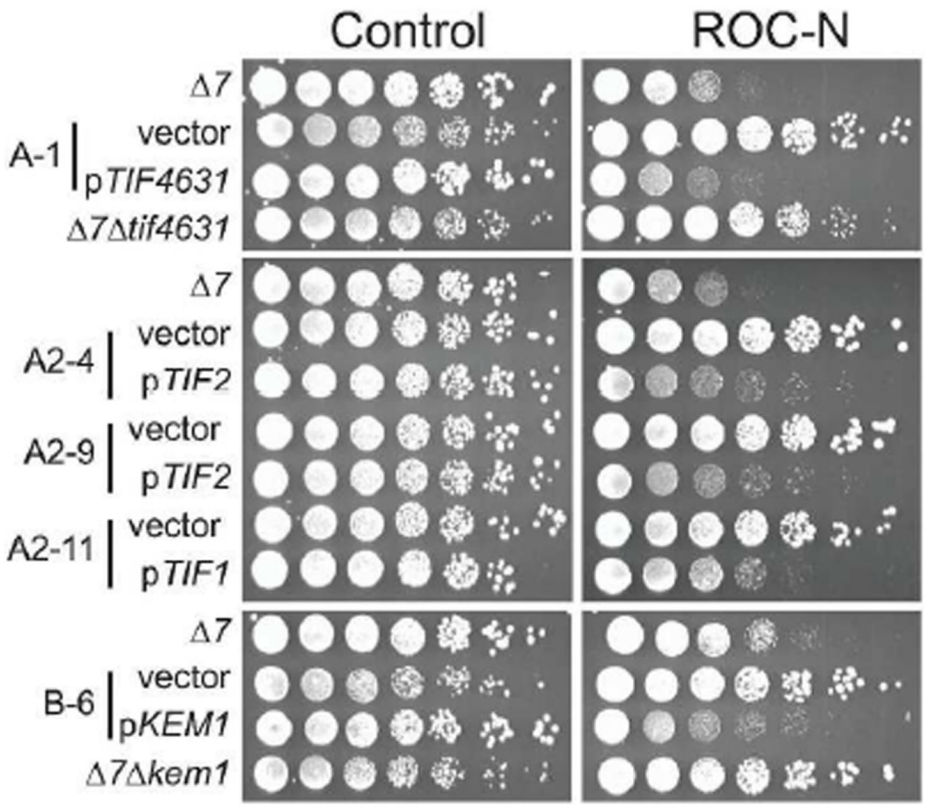

Figure 2.

Mutagenesis screening identifies three complementation groups showing resistance to ROC-N. **A.** Annotation of gene targets found mutated for individual clones within each complementation group. **B.** Sensitivity of strains from the indicated complementation classes to growth inhibition by ROC-N. Serial dilutions of individual strains were spotted onto minimal media with or without ROC-N (0.7 μM). Note that the parental strain (Δ*7*) lacks key drug resistance mechanisms, resulting in increased sensitivity to the compound (see Methods). Selected haploid resistant clones demonstrated increased ability to form colonies in the presence of compound as compared to the parental strain. Complementation

of the mutant strains with a plasmid-borne (pRS416) wild-type ORF restores compound sensitivity. Replacement of the TIF4631 and KEM1 ORFs in the Δ*7* background also leads to increased survival to ROC-N.

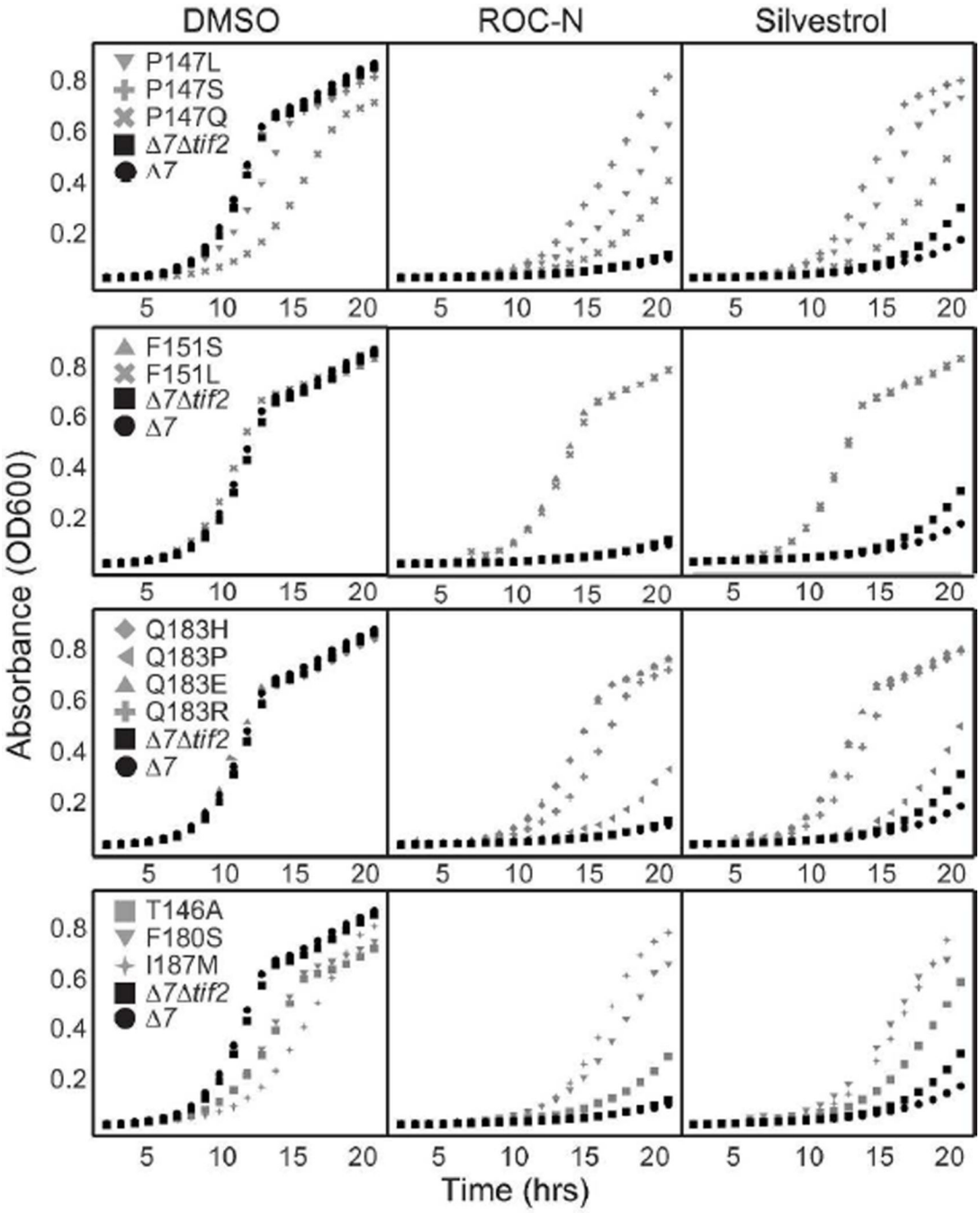

Figure 3.

Mutation at a discrete set of amino acids provides resistance to silvestrol and ROC-N. Haploid yeast strains carrying a single mutated TIF1 allele in a Δ*7*Δ*tif2* background were grown in liquid culture supplemented with DMSO (left panels), ROC-N (0.7 μM, middle panels), or silvestrol (65 μM right panels). Growth was monitored by the Absorbance at 600 nM and measured over time.

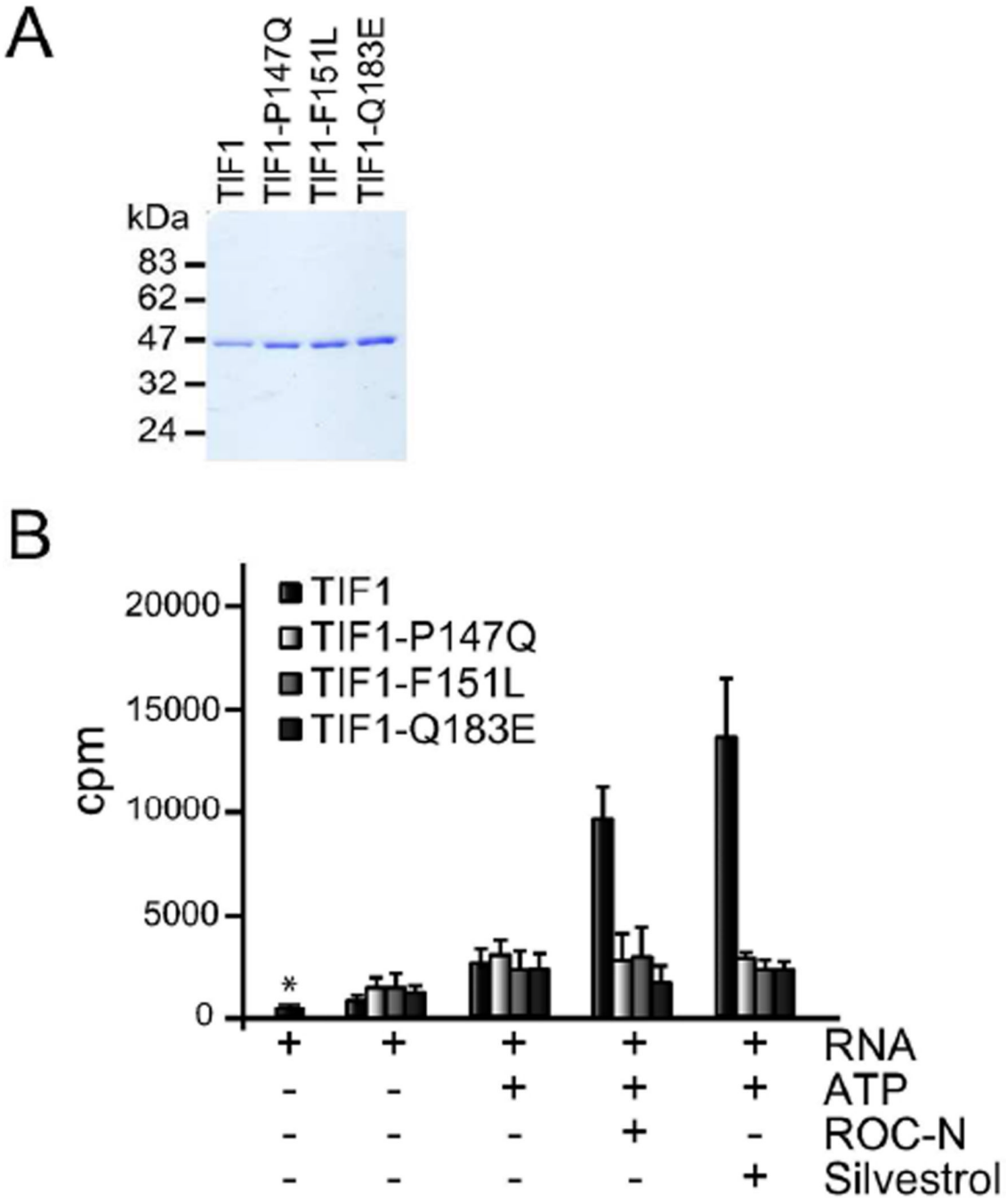

Figure 4.

Effect of TIF mutations and rocaglamides on RNA binding activity. **A.** SDS-PAGE analysis of purified recombinant TIF1 proteins. One microgram of each wild-type and mutant proteins were separated by SDS-PAGE and stained with Coomassie blue. **B.** RNA binding activity of TIF1 mutants. Asterisk denotes RNA control in the absence of protein. Assays were performed as described in the Methods in the presence of 0.5 %DMSO, 10 μM ROC-N, or 50 μM silvestrol (concentrations chosen based on the ability to block translation (Figure 1C and data not shown). n=3 ± SEM.

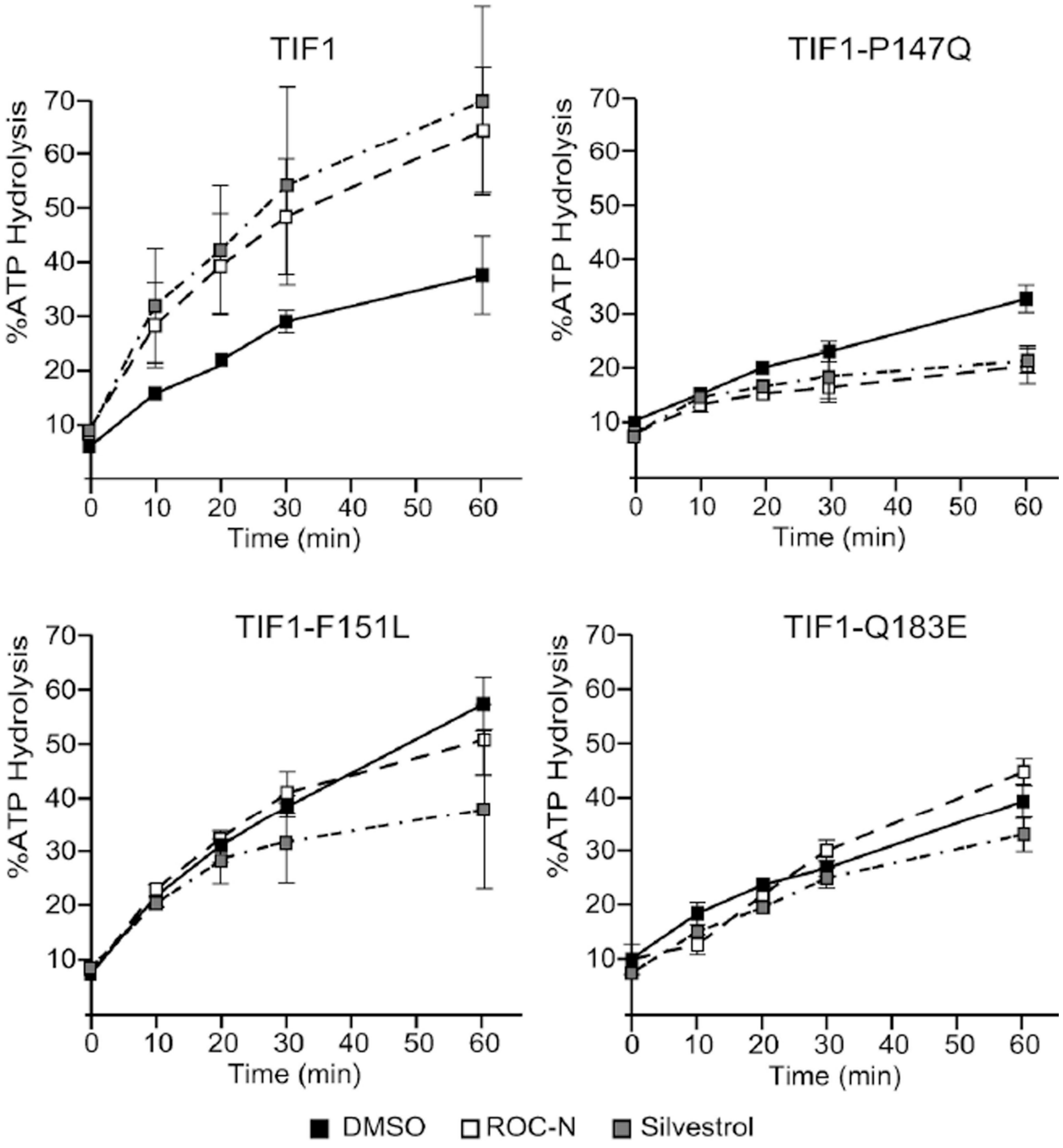

Figure 5.

Effect of TIF1 mutations and rocaglamides on ATP hydrolysis. Assays were performed as described in the Methods in the presence of 0.5% DMSO (black), 10 μM ROC-N (white), or 50 μM silvestrol (gray). The % ATP hydrolysis is plotted as a ratio of ^{32}P-Pi/(^{32}P-ATP + ^{32}P-Pi). A background value of 5 % Pi obtained in the absence of protein and RNA was subtracted from each value. n=3 ± SEM.

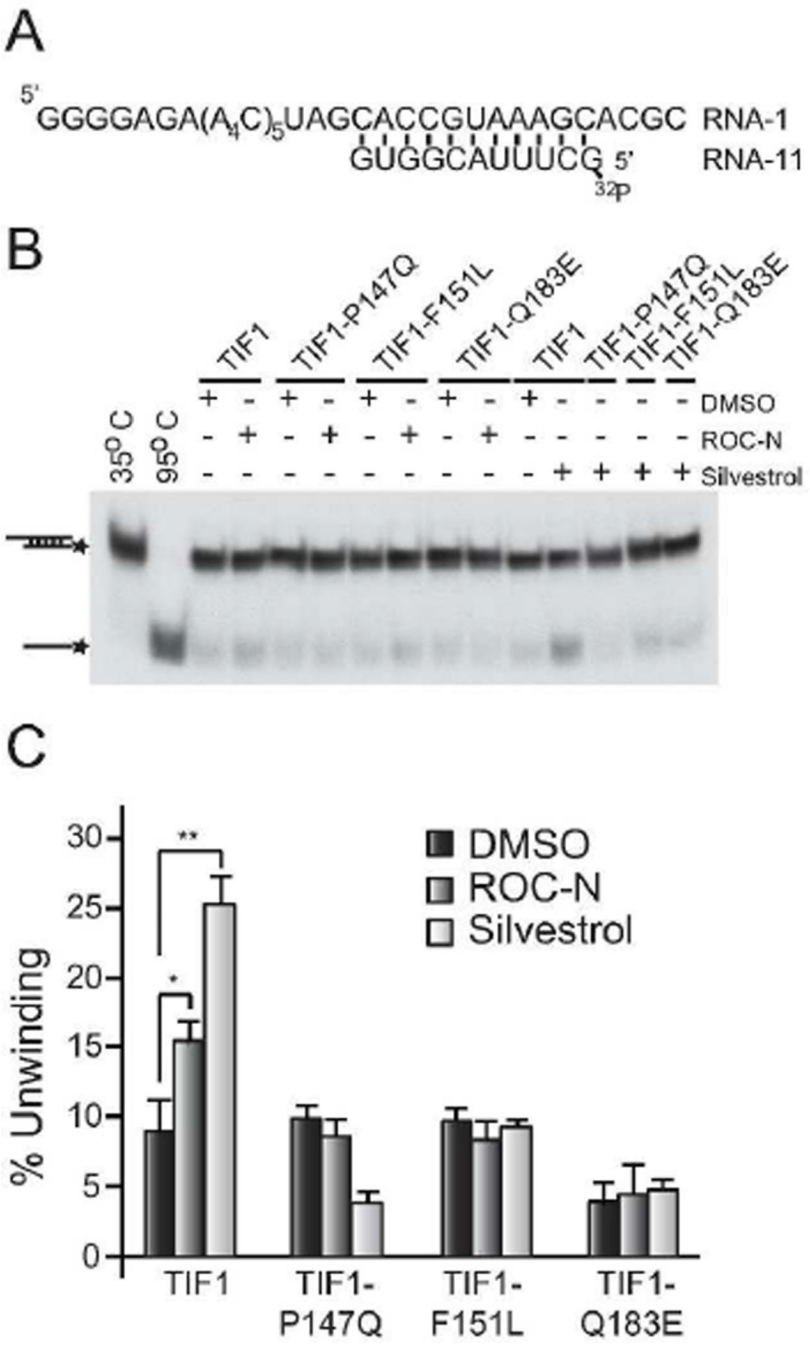

Figure 6.

Characterization of rocaglamides on RNA helicase activity of TIF1 mutants. **A.** Schematic representation of RNA substrate used in the helicase assay. **B.** Assays were performed as described in the Methods in the presence of 0.5% DMSO, 10 μM ROC-N, or 50 μM silvestrol. The position of migration of double-stranded and single-stranded RNA molecules is indicated to the left with an asterisk denoting the radiolabel. Lane 1, duplex RNA incubated under unwinding conditions without protein for 15 min at 35°C. Lane 2, duplex RNA incubated for 5 min without protein at 95°C. **C.** Quantification of TIF helicase activity. The percentage of unwinding was determined as the ratio of (monomer RNA +

duplex RNA)/monomer RNA. The percentage of monomer present in the duplex input samples (Panel B; lane 1) was set at 0% and subtracted from the values obtained in the sample lanes. n=4 ± SEM, (*p<0.05, **p<0.005).

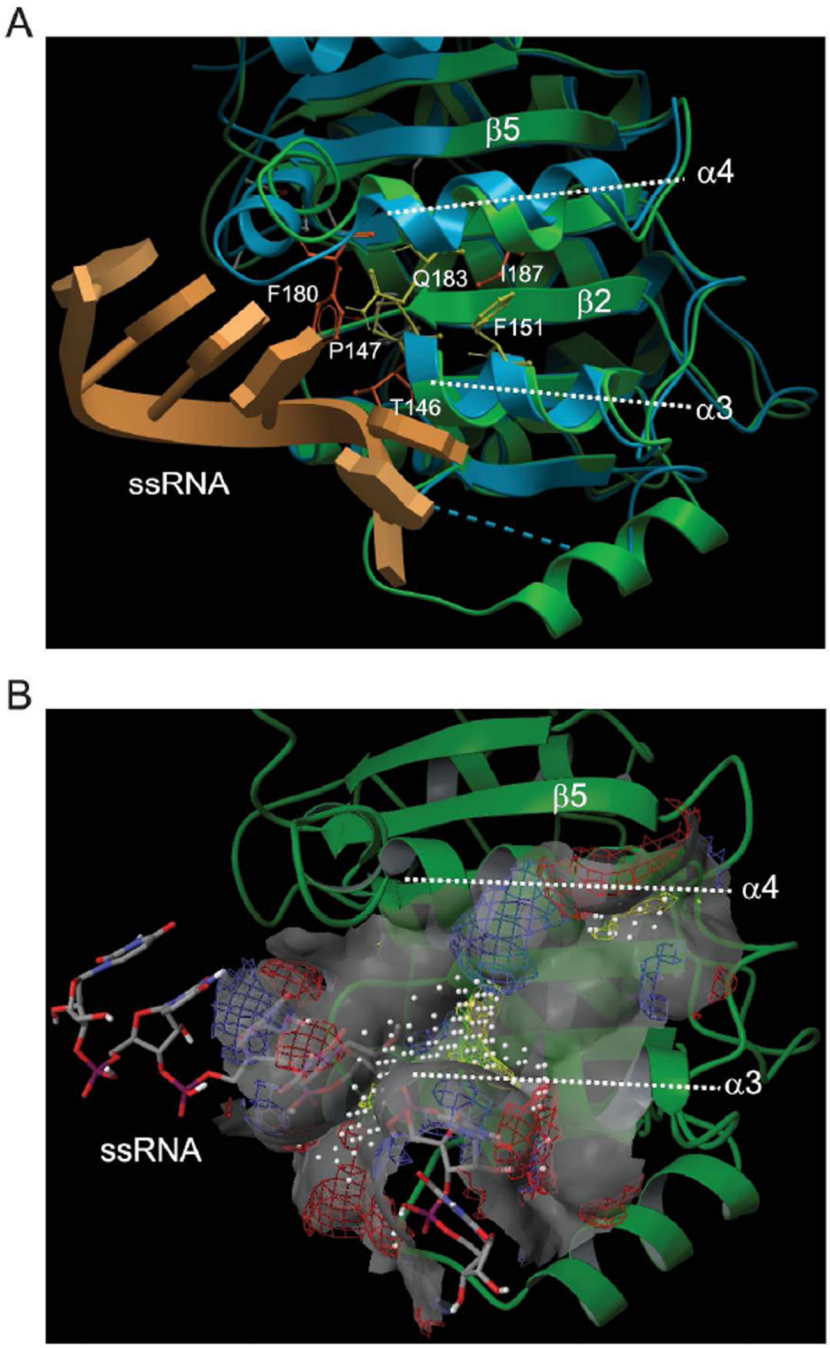

Figure 7.

In silico modeling of eIF4A homologues and putative rocaglamide binding site. **A.** Aligned ribbon diagrams of D1 domains for human eIF4AIII (PDB 2HYI, green) and yeast TIF1/2 helicases (PDB 2VSO, blue). The two domains were aligned via backbone atoms to an RMSD of 0.99A; alignment was somewhat better in the locality of helices alpha-3 and alpha-4. The RNA substrate from the eIF4AIII structure is shown in orange. TIF1/2 mutants identified in this work are highlighted in stick format and labeled, yellow for those most frequently mutated (P147, F151 and Q183) and orange for those less frequently mutated (T146, F180 and I187). Five of these residues are strictly conserved in eIF4AIII (T163,

P164, F168, F197 and Q200) whereas I187 is partially conserved as V204. **B.** The same region of the eIF4AIII helicase D1 domain visualized in **A.**, RNA substrate visualized as colored sticks. The described SiteMap sites are highlighted in grey surface rendering, with individual hydrophobic (yellow) and hydrophilic (red and blue) features outlined with colored grids; white dots represent site points used by SiteMap software to identify and merge adjacent sub-pockets (DScore of 1.02).

Table 1

Mutations in TIF1 enable resistance to ROC-N and silvestrol. IC_{50} values for individual strains were calculated at the peak of the logarithmic growth phase.

Yeast Residue	Resistant amino acid	ROC-N IC50 (μM)	Silvestrol IC50 (μM)
Thr146	Ala	0.35	65.33
Pro147	Gln	0.40	>200
Pro147	Ser	0.42	68.20
Pro147	Leu	0.53	>200
Phe151	Ser	1.03	>200
Phe151	Leu	0.87	>200
Phe180	Ser	0.68	>200
Gln183	His	0.73	>200
Gln183	Pro	0.20	38.83
Gln183	Glu	0.72	>200
Gln183	Arg	0.48	>200
Iso187	Met	13.20	>200
Δ*7*Δ*tif2*		0.18	34.64
Δ*7*		0.25	55.53